ICANS IX

INTERNATIONAL COLLABORATION ON ADVANCED NEUTRON SOURCES

22-26 September, 1986

THE IPNS RESONANCE DETECTOR SPECTROMETER*

R. K. Crawford
Argonne National Laboratory
Argonne Illinois, 60439 USA

1. INTRODUCTION

A pulsed spallation neutron source produces large quantities of neutrons with energies in the range of 1-10 eV. Time-of-flight measurements based on the pulsed nature of the source provide the basis for one energy analysis involving these neutrons, but to do spectroscopy with such neutrons a second energy analysis is required. Traditional methods such as neutron choppers or crystal Bragg reflection do not work well for such high energy neutrons, so new techniques will have to be developed if these neutrons are to be exploited for spectroscopy.

One promising technique is to make use of nuclear resonance absorption of the neutrons. A number of materials have sharp resonances, and these can be used to provide one of the energy analyses required. Resonance absorption in thin foils of absorber material can be used in either of two ways. In the first method (resonance filter method), the foil is placed in the incident or scattered beam and the resulting scattering spectrum from the sample is measured. These measurements are then repeated with the foil removed from the beam, and the results of the first measurement are subtracted from the results of the second measurement to provide a "difference" spectrum which corresponds to having only neutrons of the resonance energy in the beasm in which the foil was placed. In the second method (resonance detector method), the foil is placed in the scattered neutron beam and scattered neutrons having the resonance energy are detected "directly" by detecting the capture gammas resulting from the resonance absorption of the neutrons. The resonance filter technique has been reviewed elsewhere[1], and will not be discussed further here.

*Work supported by the U.S. Department of Energy

A prototype resonance detector spectrometer called the Electron Volt Spectrometer (EVS) has been built and operated at IPNS to gain experience with the technical problems involved in such spectrometry. One of the primary scientific reasons for using such high energy neutrons is to satisfy the kinematic requirements for measurements involving large energy transfers and small momentum transfers, such as are important in the study of magnetic phenomena. In addition to requiring large neutron energies, such measurements also dictate that the scattering angles be small. For this reason the EVS has focussed on scattering at small angles to date. [Some tests have also been made using larger scattering angles (up to 45°) for momentum distribution measurements. These have shown some promise, but are only in a preliminary stage and will not be discussed here.] In the following sections, this instrument will be described, the current understanding of the background in the instrument will be discussed, software developed to simulate the detector efficiency will be described and compared with experimental results, and a test of the use of foil-thickness difference techniques to improve resolution will be presented.

2. DESCRIPTION OF INSTRUMENT

The EVS is a "resonance detector" spectrometer, which operates by detecting promptly-emitted gamma rays resulting from resonant absorption of scattered neutrons in thin absorbers. Closely-coupled gamma ray detectors register the gamma rays, and a computer sorts the resulting pulses according to incident neutron time-of-flight. When a narrow nuclear resonance is used, this resonant capture defines the scattered neutron energy to a fixed value $E_f = E_R$ within the (practical, doppler-broadened) width of the resonance. The time-of-flight t in this spectrometer scans the scattering probability as a function of the incident energy E_i according to

$$\begin{aligned} E_i(t) &= (m/2)\,[L_i/(t - t_f)]^2 \\ E(t) &= E_i(t) - E_R \\ t_f &= L_f(m/2E_R)^{1/2} = \text{constant} \end{aligned} \tag{2.1}$$

where m is the neutron mass and L_i and L_f are the lengths of the incident and scattered neutron flight paths. Several discussions of instruments of this type have appeared in the literature[1-7].

Figure 1 shows the actual configuration of the EVS at IPNS, and Table I gives some of the parameters of this spectrometer. Two different detector geometries for small scattering angles have been used on the EVS, a closely-coupled poorly-shielded geometry (called configuration 1 throughout this paper) and a loosely-coupled well-shielded geometry (called configuration 2 throughout this paper. These are indicated in Table I and are shown respectively in Figs. 2 and 3. The kinematic range of the spectrometer for these small scattering angles is indicated in Fig. 4.

The EVS was designed to detect the gammas from the resonance foil with several separate scintillation detectors, to test the possibility of using gamma coincidence detection techniques to reduce the effects of the inescapable gamma background present. In most tests to date, 8 separate scintillation detectors were used. The data collection system allows the simultaneous collection of events from the individual scintillators ("singles" events), as well as collection of events corresponding to a coincidence (within ~0.5 μsec) between two or more individual scintillator events. A pulse-height analyzer is used to tune the gains on the amplifiers for the individual scintillators and to set the pulse-height discrimination window for each scintillator to correspond to the desired gamma energy window.

3. COLLIMATION AND BACKGROUND

3.1 Collimation

The collimation system for the EVS consists of a series of collimation elements made of lead shot and borax cast in epoxy resin (sufficient resin to fill all voids between the lead shot), alternating with B_4C cast in epoxy resin (minimal resin content). According to Table I, the unscattered neutron beam at the foil position had a penumbra diameter of 3.75 cm and an umbra diameter of 1.84 cm. The inside diameter of the resonance foil was 5.08 cm. With no scattering sample, there was no evidence of a peak at any of the Ta resonances up to 30 eV, which was the extent of the measuring range normally used. Movement of the foil off center indicated a "sharp" beam edge where the resonance peaks suddenly began to be observed. This coincided roughly with the first interception of any part of the foil with a beam penumbra of this calculated diameter. Thus the beam in the EVS has very "clean" edges, indicating that the collimation is quite good, at least at energies up to 30 eV.

3.2 Background - Coincidence Effects

For a random singles background count rate of I_{1B} counts/sec/one-μsec channel, the expected count rate using 2-fold coincidence among 8 scintillators should be reduced to

$$I_{2B} = \left(\frac{N-1}{N} \right) I_{1B}^2 \left(\frac{\tau}{r\ \Delta t} \right) \tag{3.1}$$

where τ is the allowed coincidence time window in sec, r is the pulsed source repetition rate, and Δt is the channel width (1 μsec here). Figure 5 shows "singles" (sum of events from the 8 individual scintillators) and coincidence spectra for a typical run with the detector in configuration 1 and with a polyethylene sample. For this run the singles background count rate (in 8 scintillators) was 9.0×10^{-3} counts/sec/one-μsec channel. Based on this argument (with $\tau = 0.5 \times 10^{-6}$ sec, $\Delta t = 1 \times 10^{-6}$ sec, and r = 30 Hz) the coincidence background should have been reduced to 1.2×10^{-6} counts/sec/one-μsec channel, while the measured coincidence background was 7.5×10^{-5} counts/sec/one-μsec channel. The signal-to-background ratio (signal is taken as peak height minus background level) in this singles spectrum is ~2.5, while in the coincidence spectrum it is ~12. Thus, although the signal-to-background ratio was significantly improved by using the coincidence technique, the improvement was not nearly so much as might have been expected based on an uncorrelated gamma background.

A possible explanation is that there must be one or more sources of correlated (two or more gammas produced essentially simultaneously) gammas fairly near to the detector. To a good approximation for such a source placed some distance from the N detecting scintillators, the probability of single gamma detection is

$$P_{1B} \simeq N\ \nu_B\ \varepsilon_B \tag{3.2}$$

where ε_B is the solid angle subtended at this source by a single scintillator, divided by 4π, and ν_B is the average number of coincident gammas produced by this source. Similarly, the probability of 2-fold coincidence among the N scintillators is approximately

$$P_{2B} \simeq [N(N-1)/2]\ \nu_B\ (\nu_B - 1)\ \varepsilon_B^2 \tag{3.3}$$

(Eqs. 3.2 and 3.3 are simplified versions of Eq. 4.10 below, with ε small and m = k.) Based on this argument the ratio of background counts between the singles and coincidence spectra in Fig. 5 could be accounted for if all

the background were due to a source producing an average of two gammas in coincidence at a distance of about 50 cm from the detector. Of course this is only a rough estimate of the actual distance to the correlated source or sources, since not all of the singles or coincidence backgrounds need necessarily come from such correlated sources.

Likely candidates for such a source are readily apparant in Fig. 1, namely the neutron scattering sample and the collimator just upstream from it, as well as the chamber walls and shielding aperatures around the beam between the sample and detector. All materials have some cross-section for neutron absorption, and some of these absorptions will lead to capture gamma production just as does the resonance absorption in the detector foil. In addition, neutrons scattered in all directions by the sample or collimator may be absorbed in any nearby materials, producing similar results. In this "close-coupling" geometry of configuration 1 (see Fig. 2), the scintillators have a straight "line-of-sight" to the sample, and it is not possible to place any significant gamma absorber in this path without introducing intolerable attenuation of the scattered neutrons we wish to detect. For this reason, the "well-shielded" configuration 2 geometry shown in Fig. 3 was considered. This arrangement makes use of the same resonant foil and the same bismuth germanate (BGO) scintillator crystals used in the first geometry, but moves the scintillators to well-shielded locations around the periphery of the foil. As a consequence, the scintillators subtend smaller solid angles for detecting gamma events in the foil, reducing the overall detection efficiency of the detection system.

Figure 6 shows singles and coincidence spectra from this same polyethylene sample, this time collected with the detector in configuration 2. For this run the singles background count rate was 6.0×10^{-4} counts/sec/one-μsec channel and the coincidence background was 5.0×10^{-6} counts/sec/one-μsec channel. The signal-to-background ratio in this singles spectrum is ~17.5, while in the coincidence spectrum it is ~25. Based on the above analysis, the coincidence background for a random gamma flux in this case should have been 5.3×10^{-9} counts/sec/one-μsec channel. Thus the new configuration significantly reduced the background and improved the signal-to-background ratio, but the remaining background is even more highly correlated than was the background in configuration 1. The sources of this background are discussed further in Section 3.3 below.

Figure 7 shows the singles spectrum for a vanadium sample with the detector in configuration 2. In this case where the sample scattering is much weaker and is not peaked in the forward direction as it is for scattering from hydrogen, and where the sample absorption is strong, the signal-to-background ratio is much worse. The background in the singles spectrum for this sample is 5.3×10^{-4} counts/sec/one-μsec channel, and the singles signal-to-background ratio is ~3.7. Due to the much lower scattering power, it was not possible to get coincidence data for this sample in a reasonable measurement period.

3.3 Background - Filter Measurements

A series of runs were made in configuration 1 and configuration 2 with lead, iron, and beryllium filters in the beam upstream from the sample. These filter materials were chosen to provide transmissions which would discriminate between gammas, high energy neutrons, and low energy neutrons in the incident beam, in an attempt to pinpoint the source of the measured background. For each type of filter material, a "transmission" was calculated based on the measured beam monitor data, according to the expression

$$\text{Transmission} = \frac{\text{Bkgnd with Filter} - \text{Bkgnd with Gate-closed}}{\text{Bkgnd with No-filter} - \text{Bkgnd with Gate-closed}} \quad (3.4)$$

where data from all runs has been normalized on the same basis (pulses, or pulses combined with beam current). A similar "transmission" was calculated using the measured singles data both with and without a polyethylene sample in the beam for both configurations, and for configuration 2 with a vanadium sample as well. The results of these "transmission" measurements can be accounted for by assuming the background is made up of the following components:

A. A background component due to ~ 4 MeV gammas coming down the beam and interacting with something other than the sample.

B. A background component due to ~ 4 MeV gammas coming down the beam and interacting with the sample.

C. A background component due to ~ 100 keV neutrons coming down the beam and interacting with something other than the sample.

D. A background component due to ~ 100 keV neutrons coming down the beam and interacting with the sample.

E. A background component due to non-beam sources.

Using this 5-component model to compare the measured "transmission" data with the expected transmissions of these filter materials for neutrons[8] and gammas[9] of various energies, it was possible to calculate the relative magnitudes of each of these components in the background for each detector configuration. These results are shown in Table II. Table II shows a factor of about 20 reduction in most of the background components in going from configuration 1 to configuration 2. Component A was reduced much more, however (at least a factor of 1000). This Table shows that for flight times around 350 μsec the overall reduction in the background was roughly a factor of 20, but that at times around 100 μsec the reduction was much greater. These considerations seem to indicate that while some of component A was present at the longer times, most of component A was concentrated at the shorter times. Thus while Table III shows a "total" background reduction factor of 33 between the two configurations, the background in the region of interest around 300-400 μsec was reduced by only a factor of about 20.

4. CALCULATED AND MEASURED DETECTOR EFFICIENCY

4.1 Calculation of Detector Efficiency

The neutron detection process in a resonance detection system such as that on the EVS has four major components. These are:

1) resonant absorption of the neutron in the resonance foil

2) production of prompt gamma cascades by decay of the compound nucleus formed in step 1)

3) interception of one or more of these gammas by individual scintillators around the resonance foil

4) detection of these gammas by the scintillator detector systems

In order to understand the performance of the various prototype detector geometries well enough to design an improved detector system, software has been developed to simulate each of these independently, as well as to look at the combination of components 2) and 4). Although the four components are not all strictly independent (eg - the number of gammas formed in a cascade is correlated with their energies, leading to a correlation of the number of gammas with their detection probabilities in the scintillators), only the correlations between components 2) and 4) are sufficiently strong to require their simultaneous treatment. When it comes to predicting the

performance of different detector configurations, separate approximate treatment of the effects involved in each process is much more illuminating than would be a more accurate calculation in which all effects are treated together to allow for correlations. Therefore, the software packages for the various processes have been kept separate so far, rather than combining them into a single package. The various processes are discussed below.

4.2 Resonant Absorption of Neutrons

The resonance absorption cross-section σ'_{abs} for neutrons in the center-of-mass system is described by the Breit-Wigner formula[10,11]

$$\sigma'_{abs} = (h^2/8\pi mE')\, g_J \, \frac{\Gamma_n \Gamma_r}{(E'-E_R)^2 + (\Gamma/2)^2} \tag{4.1}$$

$$\Gamma = \Gamma_n + \Gamma_r \tag{4.2}$$

where h is Planck's constant, Γ_n, Γ_r, and Γ are the neutron width, the radiative capture width, and the total width of the resonance centered at the center-of-mass energy E_R, g_J is a statistical spin factor, and E' is the energy of relative motion of the neutron and target nucleus in the center-of-mass system.

In any real resonant absorber, the cross-section σ_{abs} in the laboratory system depends also on the motion of the resonantly absorbing nuclei, so the cross-section expression given above must be modified to account for this "doppler broadening". It can be shown[11,12] that a reasonably accurate treatment is to take the effective cross-section in the laboratory to be the center-of-mass cross-section given by Eq. 4.1 convoluted with a gaussian of standard deviation $\Delta/\sqrt{2}$, where

$$\Delta = (4mEkT^*/M)^{1/2} \tag{4.3}$$

with E the neutron energy in the laboratory, M the mass of the target nucleus, and

$$kT^* \simeq (3k\theta_D/8)\coth(3\theta_D/8T) \tag{4.4}$$

(The approximation 4.4 is justified only for high temperatures[11], but in fact it is quite a good approximation throughout the temperature range.)

The program FOIL accepts input parameters for one or more resonance foils and for one or more resonances per foil. From these it calculates T^*

using Eq 4.4, Δ using Eq. 4.3, and numerically performs the gaussian convolution with Eq. 4.1 to get σ_{abs}. It also calculates the absorption probability $p_A(E)$ for the foil according to

$$p_A(E) = 1 - e^{-\sigma_{abs}(E)\, d} \tag{4.5}$$

where d is the foil thickness in units of absorbing nuclei per cm^2. Figure 8 shows calculated absorption probabilities for the 4280 meV Ta resonance for three different thicknesses of foil, based on the known resonance parameters[13] and other data for Ta metal at 300 K. In this figure one can clearly see the strong wings due to the intrinsic Lorentzian shape of the resonance line (doppler effects produce significant modifications only near the peak). These wings are significant at energies of several hundred meV away from the resonance peak, and will lead to difficulty in measuring weak inelastic peaks at energy transfers below about 500 meV when the Ta (or any other) resonance is used in a resonance detector spectrometer.

4.3 Production of Gamma Cascades

When a slow neutron is absorbed by a heavy nucleus of mass A, an excited nucleus of mass A+1, sometimes called a compound nucleus, is formed. This nucleus has an energy which is an amount U_o above the ground state, where U_o is the binding energy of the neutron in the compound nucleus. For most heavy nuclei, U_o is about 6-7 MeV. For the nuclei of interest, the dominant method of de-excitation of this excited nucleus is by prompt gamma decay. Depending upon the selection rules for the particular compound nucleus, the initial decay may be directly to the ground state of the nucleus, or to any of a large number of excited states of this nucleus. If the decay is to a lower-energy excited state, this state usually can itself decay via prompt gamma emission. The net result of such a neutron capture is then a cascade of prompt gammas[14], occurring within about 10^{-14} sec, with the total energy of these gammas adding up to the initial excitation energy U_o.

The statistical model of cascade gamma production was first formulated by Blatt and Weisskopf[10], and has been used by a number of authors[15-18] to calculate gamma spectra of heavy nuclei. In this model, the nuclear energy levels are assumed to be distributed continuously according to a "statistical" distribution. The derivations and assumptions involved in the various uses of this model were summarized by Lynn[11], who also reviewed some

of the efforts to fit the experimental spectra using this model. The program GAMMA incorporates a "Monte Carlo" computational scheme based on the statistical model to generate gamma cascades between the energy U_o and the ground state. Figure 9 shows a cascade gamma spectrum calaulated using this statistical model Monte Carlo approach with the "best" choice of the one adjustable parameter in the model. Also shown is an experimental measurement[19] of the cascade gamma spectrum for Ta. As seen in Fig. 9, the calculated curves reproduce the experimental spectrum quite well for gamma energies above about 0.8 MeV. The calculations start to diverge from the experimental data at lower energies, which is where the statistical theory is expected to break down. For gamma energies above about 0.8 MeV, the statistical model appears to be a fairly good model of the actual cascade process in Ta.

The program GAMMA also calculates the probability f_ν of having a given number ν of gammas with energies within a selected window in a cascade, and this is tabulated in Table III. The quantity f_ν is strongly dependent on the energy window used for gamma selection. However f_ν is not strongly dependent on details of the level densities assumed in the model, so at least for gamma energy windows with lower limits above about 0.8 MeV the program GAMMA should give fairly good values for f_ν. (Note that the average total number of gammas per cascade in Table III comes out to be about 4, also in good agreement with earlier statements[6].)

4.4 Gamma Detection in Scintillator Crystals

The pulse height of the output pulse from the photomultiplier-preamp combination coupled to a scintillator is proportional to the light output by the scintillator (assuming good optical coupling), and this in turn is proportional to the energy deposited in the scintillator. Thus pulse-height discrimination on the output pulses can be used as a means of selecting only those events resulting in energy deposition values within a preselected range. The net undisturbed transmission of gamma rays of energy E through a thickness d of a material is given by[20]

$$I(E) = I_o(E)\, e^{-\mu(E)d} \qquad (4.6)$$

where the total linear attenuation coefficient $\mu(E)$ is given by

$$\mu(E) = \sum_i n_i [\sigma_{ph}(E) + \sigma_c(E) + \sigma_{pp}(E)]_i$$

$$= \mu_{ph}(E) + \mu_c(E) + \mu_{pp}(E) \qquad (4.7)$$

Here $\sigma_{ph}(E)$, $\sigma_c(E)$, and $\sigma_{pp}(E)$ are the atomic cross-sections for photoelectric absorption, compton scattering, and pair production for gammas of energy E in atoms of type i, and n_i is the number density of atoms of type i in the material.

A Monte Carlo routine SCNTDET has been developed to follow a gamma along its path in a scintillator until it and/or all lower energy gammas produced in the scintillator either deposit all their energy or leave the scintillator. In the process, this program keeps track of the energy deposited. The program contains detailed cross-section information for the various gamma-interaction processes[21], which is used to determine the point and type of interaction of a gamma within the scintillator according to the probability distribution given by Eqs. 4.6 and 4.7. This program has been tested against published pulse-height data[22] for NaI scintillators in specific geometries, with good agreement.

Table IV shows data generated by the program GAMMA, similar to the data in Table III. However, in Table IV, the routine SCNTDET has been used within GAMMA to select only those gammas which would be detected by 2.5 cm diameter by 2.5 cm long BGO scintillators in configurations similar to those encountered in detector configuration 2 (gamma source on cylinder side at midplane, 4.3 cm from cylinder center). Comparison of Tables III and IV shows an enormous difference in the probability distributions f_ν for production and f_ν' for detection (with pulse-height discrimination) of ν gammas. A large number of the gammas are missed by the detector because they deposit less than their full energy in the scintillator. This points out that an obvious improvement in the detector system would be to use larger scintillators to improve the probability of interaction of both the primary gamma from the resonance foil and of the secondary gammas (compton scattering or electron-positron anihilation) produced within the scintillator.

4.5 The Effects of Discrete Gamma Detectors - Coincidence Probabilities

As discussed above, a single neutron capture results in the production of several gammas of varying energies, and for present purposes these can be regarded as being produced simultaneously with no angular correlation among

them. If ν detectable (ie - will be detected if they are directed toward a scintillator) gammas are produced within the detector energy acceptance window in such an event, then the evaluation of $P(\nu,k)$, which is the probability that k or more of these gammas will impinge upon exactly k separate scintillation detectors, is just a counting problem. If ε_i is the fraction of the total solid angle subtended by the i^{th} scintillator at the gamma-producing event, and there are N scintillators, then

$$P(\nu,k) = \sum_{m=k}^{\nu} P_m(\nu,k) \tag{4.8}$$

where $P_m(\nu,k)$ is the probability that exactly m gammas will impinge on exactly k scintillators under these conditions. Evaluation of $P_m(\nu,k)$ gives

$$P_m(\nu,k) = C_m^{\nu} \left(1 - \sum_{j=1}^{N} \varepsilon_j\right)^{\nu-m} \left[\sum_{l_1=0}^{m}{}' \cdots \sum_{l_N=0}^{m}{}' \varepsilon_1^{l_1} \varepsilon_2^{l_2} \cdots \varepsilon_N^{l_N} T_{ml} \right] \tag{4.9}$$

where

$C_m^{\nu} = \dfrac{\nu!}{m!(\nu-m)!}$ is the number of ways m gammas can be selected from ν total

$\left(1 - \sum_{j=1}^{N} \varepsilon_j\right)^{\nu-m}$ is the probability that ν-m gammas are not detected

$\left[\sum_{l_1=0}^{m}{}' \cdots \sum_{l_N=0}^{m}{}' \varepsilon_1^{l_1} \cdots \varepsilon_N^{l_N} T_{ml} \right]$ is the probability of detecting the remaining m gammas in exactly k scintillators with at least one in each of the k scintillators

$\sum_{l_1=0}^{m}{}' \cdots \sum_{l_N=0}^{m}{}'$ sums are constrained so that $\sum_{i=1}^{N} l_i = m$ and exactly k of the l_i are non-zero

$T_{ml} = \dfrac{m!}{l_1! l_2! \cdots l_N!}$ is the number of ways the m gammas can be arranged in the N scintillators with a particular set of occupation numbers $\{l_i\}$

For a special case, namely all ε_i the same, Eqs. 4.8 and 4.9 reduce to the simplified form given by Muradyan[23]

$$P'(\nu,k) = \sum_{m=k}^{\nu} C_m^{\nu} (1-N\varepsilon)^{\nu-m} \varepsilon^m C_k^N \left[k^m + \sum_{t=1}^{k-1} C_t^k t^m (-1)^{k-t}\right] \tag{4.10}$$

In practice, if ε is small only the term m = k is significant. Although this special case is almost never exactly satisfied, this simplified form is quite useful for estimating the magnitude of effect which will result from changing the detector geometry[6].

The actual probability of detecting a gamma in at least one scintillator ("singles" probability) when a neutron is absorbed in the resonance foil is

$$P_1 = \sum_{\nu=1}^{\nu_{max}} \sum_{k=1}^{\nu} \langle P(\nu,k) \rangle f_\nu' = \sum_{\nu=1}^{\nu_{max}} P_{1\nu} \qquad (4.11)$$

where < > means average over all possible event positions within the resonant foil, and f_ν is the fraction of neutron absorptions which result in exactly ν detectable gammas with energies within the acceptance window for the scintillation detectors. Similarly, the probability of detecting gammas in coincidence in two or more scintillators ("2-fold" coincidence probability) is

$$P_2 = \sum_{\nu=2}^{\nu_{max}} \sum_{k=2}^{\nu} \langle P(\nu,k) \rangle f_\nu' = \sum_{\nu=2}^{\nu_{max}} P_{2\nu}$$

$$= P_1 - \sum_{\nu=1}^{\nu_{max}} \langle P(\nu,1) \rangle f_\nu' \qquad (4.12)$$

Table V shows values of P_1 and P_2 calculated for the two detector configurations and for different discriminator energy windows. These tabulated values are based on the values for P(ν,k) obtained from Eqs. 4.8 and 4.9 using the program DETPROB, together with the values for f_ν' from Table IV.

4.6 Experimental Tests of Calculated Detector Efficiency

The calculated detector efficiency can be compared with the measured data rates for the runs shown in Figs. 5-7. For the polyethylene sample, the total number of hydrogens in the beam was $N_H = 5.6 \times 10^{22}$, and assuming a total cross-section of 20 barns for H the laboratory-frame scattering[24,25] at small angles from this sample can be reasonably estimated as $N_H(d\sigma_H/d\Omega)_{lab} = 0.36$ cm^2/sr. For the vanadium sample, the number of atoms in the beam was roughly $N_V = 1.3 \times 10^{23}$, giving $N_V(d\sigma_V/d\Omega)_{lab} = 0.050$ cm^2/sr.

The measured flux from a 100 cm^2 polyethylene moderator in the F position at IPNS is[26]

$$EI_p(E) \simeq 3 \times 10^{10} (A_{source}/100) \quad \text{neut/sr-}\mu\text{A-sec} \qquad (4.13)$$

at E = 1 eV. Since this is the epithermal region, $I_p(E)$ should vary as 1/E. Using a source current J_s = 12 μA, a channel width Δt = 1 μsec, and an elastic scattering energy of E = 4280 meV giving an elastic flight time of t = 384 μsec, with other data from Table I, gives

$$\Phi_s(t)\,\Delta t = [EI_p(E)]_{1\ eV}\,(1/E)\,J_s\,(1/L^2)\,(2E/t)\,\Delta t$$
$$\simeq 470 \quad \text{neutrons/cm}^2\text{-sec-chan} \qquad (4.14)$$

as the number of neutrons incident on the sample per unit area per unit time per one μsec channel at the detector, for a neutron energy of 4280 meV.

Using the above values and data from Table I, the number of neutrons on the detecting foil with the polyethylene sample should be

$$I_{pf}(t)\,\Delta t = \Phi_s(t)\,\Delta t\,\Delta\Omega \left(N_H \frac{d\sigma}{d\Omega}H\right)_{\phi_{lab}}$$
$$\simeq 1.02 \quad \text{neutrons/sec-chan} \qquad (4.15)$$

and for a vanadium sample it should be

$$I_{vf}(t)\,\Delta t \simeq 0.143 \quad \text{neutrons/sec-chan} \qquad (4.16)$$

Table VI shows the measured singles and coincidence data rates (minus background) for the peak channel in the 4280 meV elastic peak in the spectra in Figs. 5-7. Also shown in the table are the corresponding rates calculated using Eqs. 4.15 or 4.16 for the number of neutrons on the detector foil, along with the data in Table V for the detector efficiency per neutron absorbed in the foil, and data from Fig. 8 for the foil absorption probability for a 12.5 micron thick Ta foil (used for configuration 1 measurements) and for a 7.5 micron thisk Ta foil (used for configuration 2 measurements).

As seen in Table VI, the absolute data rates measured in the singles peaks were lower than the calculated values by factors ranging from ~2 (vanadium, configuration 2) to ~4 (polyethylene, configuration 1). However the calculated ratios between singles and coincidence data rates agreed fairly well (within ~25%) with the measured ratios for both configurations.

The discrepancies between the calculated and measured values for absolute data rates can be due to the values used for the incident neutron flux, for the sample scattering probability, for the absorption efficiency of the foil, for the gamma production per foil absorption, or for the gamma detection efficiency of the scintillator-photomultiplier-electronics system (eg - discriminator settings for some of the measured data might have drifted from the values used in the calculation), or a combination of these. The difference between the polyethylene and vanadium results for the same configuration indicates that at least part of the discrepancy between calculated and measured values lies in the estimation of the sample scattering, rather than in the calculations of detector performance. This is consistent with the relatively good agreement for singles-to-coincidence ratios achieved in the calculations, since these ratios do not depend on the amount of sample scattering.

4.7 Discussion of Detector Efficiency

As can be seen in Table V, the efficiency of the detector is quite low in configuration 2, with the calculated detection probability of a 4280 meV neutron incident on a 7.5 micron foil being about 2.7%. This efficiency could be improved in several ways. Increasing the resonance foil thickness would increase the probability of absorption at the peak, and hence increase the detection efficiency. However, for a 7.5 micron thick Ta foil this absorption probability is already ~0.6, so there is not much room for improvement there. Increasing the foil thickness would worsen the resolution (see Section 5 below), so this is not a desirable approach.

A much better approach would be to increase the size and number of scintillators used. Comparison of Tables III and IV shows that for reasonable pulse-height windows about 50% of the gammas produced with energies within this window do not deposit enough of this energy in the scintillators presently used to be detected. Thus a factor of nearly 2 improvement in the detection efficiency of a single scintillator is possible. In addition, the present scintillators subtend only a very small solid angle at the gamma source in the resonance foil (in detector configuration 2 on the average the 8 scintillators cover only 0.075 of the total solid angle for gamma interception) so most of the gammas produced will not hit any scintillator. With careful design it should be possible to

increase this by at least a factor of 5. To a first approximation the singles detection efficiency scales linearly with improvements in the gamma detection efficiency of a single scintillator, and also scales linearly with increases in solid angle for gamma detection, so an improvement of nearly a factor of 10 in the singles detection efficiency over that seen for the prototype detector configuration 2 should be possible. Unfortunately, to a first approximation the measured background should scale in the same manner. However, any such increases in singles detection efficiency will appear roughly squared in the coincidence detection efficiency, so increasing the scintillator size may offer significant improvement in the signal-to-background seen in the coincidence spectra, as well as improving the coincidence detection efficiency to a high enough value to make the use of this technique practical.

The tests reported here show that although there are still some problems, the detector simulation software gives sufficiently reliable results to be a useful design tool. Future efforts with this software will be directed to the study and/or design of a detector system employing large scintillators, in an effort to quantify the assertion made above about the effects of scintillator size and to arrive at an improved detector design.

5. USE OF DIFFERENCE TECHNIQUES TO IMPROVE RESOLUTION

As noted in Section 4.2, the Ta resonance is fairly broad, and has broad Lorentzian wings. However, the detection probability for a neutron is proportional to the absorption probability $P_A(E)$ of the foil, as given by Eq. 4.5, rather than to the absorption cross-section $\sigma_{abs}(E)$ alone. Thus the peak in detection probability given by $p_A(E)$ has a somewhat flatter top than does $\sigma_{abs}(E)$, due to saturation effects in the exponential in Eq. 4.5, and the extent of this saturation depends on the thickness of the absorbing foil. Figure 8 shows clearly the flattening of the peak due to saturation of the absorption as the foil thickness is increased. This latter feature can be used to good advantage to narrow the peak and to remove most of the wings. To do this, spectra are taken with two different thicknesses of foil, normalized to match in the wings, and subtracted. Such a subtraction of the calculated curves for the 7.5 micron and 25 micron Ta foils is also shown in Fig. 8. The potential improvements from this technique are quite

evident in the figures, although this improvement can only be gained with a significant increase in counting time per experiment, and then only if the background can be properly subtracted in each case. Preliminary demonstrations of the feasibility of using such difference techniques to improve resolution have been reported[1,5,6] by other investigators.

Figure 10 shows data for a sample of ZrH_2 on the EVS. The sample was placed at 10.5 m from the source and 0.5 m from the resonance foil. This made the average scattering angle ~ 4.45°, giving Q ~ 3.6 A^{-1}. Data were collected with a ~ 7.5 micron thick Ta foil, a ~ 25 micron foil made of two thicknesses of ~ 12.5 micron Ta, and with no Ta foil. The no-foil "background" run was fit with a quadratic function, and the resulting smooth background was subtracted from the 7.5 micron and 25 micron raw data to produce the curves shown in Fig. 10. Not surprisingly, the fundamental inelastic mode of the hydrogen vibration in ZrH_2 is not resolved. However, by subtracting the 25 micron data, scaled to match the 7.5 micron data in the wings as shown in Fig. 10, from the 7.5 micron data, the results shown in Fig. 11 are obtained. Also shown in Fig. 11 are the calculated results based on the relative amplitudes of the elastic peak and the various inelastic peaks predicted by harmonic oscillator theory[29] for an oscillator frequency of 140 meV (which is approximately the value for ZrH_2). In the calculation, the harmonic oscillator results have been broadened according to the 7.5 micron - 25 micron "difference resolution function" shown in Fig. 8. The overall amplitude of the calculated curve has been scaled to match the elastic peak, but there are no other adjustable parameters. Although statistics are not good enough to get a really good picture of the shape of the inelastic scattering, the elastic peak has clearly been sharpened enough by this difference technique so that the inelastic data can be resolved, and the overall magnitude of the inelastic scattering is in good agreement with the calculated value. The three data sets required a total collection time of ~ 135 hours for a sample of ZrH_2 which put ~ 2×10^{22} H atoms in the beam , with the accelerator producing an average current of ~ 12 μA. With a more efficient detector (see Section 4.7) much better statistics could be achieved in this amount of time. Thus this technique does seem to provide a practical approach to the improvement of resolution in such an instrument, at least for some types of problems.

TABLE I - Operating parameters for the EVS at IPNS.

Incident Path L_i	10 m	
Scattered Path L_f	1 m	
Resonant Foil Geometry	annular, centered on beam	
Resonant Foil Size	10.16 cm od, 5.08 cm id	
Resonant Foil Solid Angle at Sample	0.0061 sr	
Scattering Angle	1.5° - 3°	
Resonant Foil Material	Ta	
Resonance Energy E_R	4.28 eV	
Beam Diameter at Moderator - Umbra	5.65 cm	
Beam Diameter at Sample	2.54 cm	
Beam Diameter at Foil - Umbra	1.84 cm	
Penumbra	3.75 cm	
Gamma Detectors	8 BGO* cylinders 2.54 cm dia, 2.54 cm long	
	Configuration 1	Configuration 2
Gamma Detector Configuration	45° apart, centered 4.6 cm from beam center and 2.5 cm from foil	30° apart, centered 8.26 cm from beam center in plane of foil

* BGO stands for a bismuth germanate crystal directly coupled to a Hamamatsu model R268 photomultiplier.

TABLE II - Magnitudes of different contributions to the background with different samples and detector configurations. Values given are the contribution per second.

Background Source	Range(μsec)	Polyethylene Sample Config 1	Polyethylene Sample Config 2	V Sample Config 2	Config 1:2 Ratio
gamma-no sample	100-600	4.9	0.000	0.000	> 1000
gamma-sample	100-600	0.51	0.030	0.033	17
neutron-no sample	100-600	0.81	0.045	0.054	18
neutron-sample	100-600	0.72	0.108	0.195	7
non-beam	100-600	0.72	0.051	0.117	14
Total	100-600	7.6	0.234	0.399	33
Total one channel	100-101	0.098	0.0015	0.0022	65
Total one channel	350-351	0.010	0.00066	0.00051	15

TABLE III - Probabilities for production of different numbers of coincident gammas within selected energy windows, calculated using the statistical model Monte Carlo program GAMMA.

	Probability f_ν			
Number of Gammas ν		Energy Window (MeV)		
	no window	0.8-5.2	0.8-3.0	1.5-5.2
0	0.000	0.037	0.061	0.039
1	0.003	0.024	0.356	0.287
2	0.064	0.446	0.199	0.612
3	0.283	0.418	0.310	0.061
4	0.387	0.073	0.072	0
5	0.206	0.002	0.002	
6	0.051	0	0	
7	0.006			
8	0.001			
9	0			
$\bar{\nu}$	3.911	2.472	1.983	1.696

$\bar{\nu}$ = Average number produced within energy window per cascade.

TABLE IV - Probabilities for different numbers of coincident detectable gammas using scintillators with pulse-height discrimination, calculated using GAMMA and SCNTDET with gammas incident from the side on a 2.5 cm dia x 2.5 cm long BGO scintillator.

	Probability f_{ν}'			
Number of Detected Gammas ν		Discriminator Window (MeV)		
	no window	0.8-5.2	0.8-3.0	1.5-5.2
0	0.000	0.481	0.542	0.672
1	0.003	0.399	0.355	0.299
2	0.063	0.109	0.093	0.028
3	0.277	0.010	0.010	0.000
4	0.389	0.001	0.001	0
5	0.209	0	0	
6	0.052			
7	0.006			
8	0.000			
$\bar{\nu}$	3.921	0.651	0.572	0.357

$\bar{\nu}$ = Average number detected within energy window per cascade.

TABLE V - Weighted total singles and 2-fold coincidence detection probabilities for different gamma detection energy windows, calculated using detectable gamma frequency data from Table III and scintillator "hit probabilities" $P(\nu,k)$ given by DETPROB.

	Detector Configuration 1		Detector Configuration 2	
Window (MeV)	P_1	P_2	P_1	P_2
no window	0.567	0.130	0.268	0.0302
0.8 - 5.2	0.125	0.0040	0.051	0.00081
0.8 - 3.0	0.111	0.0036	0.045	0.00072
1.5 - 5.2	0.070	0.0008	0.028	0.00016

TABLE VI - Calculated and measured data rates (minus background) in the peak channel for the 4280 meV elastic peak for the runs shown in Figs. 5-7. The discriminator window for gamma detection was set to 0.8-3.0 MeV for all three runs. Calculated values are based on Eqs. 4.13 or 4.14 together with the appropriate P_1 or P_2 values from Table V and foil absorption probabilities from Fig. 8, and are in units of counts/sec/one-μsec channel.

		Singles		Coincidence		Ratio	
Config	Sample	Calc	Meas	Calc	Meas	Calc	Meas
1	polyethylene	0.091	0.023	0.0029	0.00085	31	27
2	polyethylene	0.028	0.010	0.00044	0.00012	64	83
2	vanadium	0.0039	0.0020				

REFERENCES

1. Newport, R. J., Paoli, M. P., Pugh, V. T., Sinclair, R. N., Taylor, A.D., and Williams, W. G., ICANS VIII - Proceedings of the Eighth Meeting of the International Collaboration on Advanced Neutron Sources, RAL-85-110, Rutherford Appleton Laboratory, 562-576 (1985).

2. Sinclair, R. N., Moxon, M. C., and Carpenter, J. M., Bull. Am. Phys. Soc. 22, 101 (1977).

3. Allen, D. R., Mitchell, E. W. J., and Sinclair, R. N., J. Phys E: Sci Instrum 13, 639-646 (1980).

4. Carpenter, J. M., Watanabe, N., Ikeda, S., Masuda, Y., and Sato, S., Physica 120B, 126-130 (1983).

5. Watanabe, N., Proceedings of the 1984 Workshop on High-Energy Excitations in Condensed Matter, Los Alamos, Feb. 13-15, 1984. LA-10227-C, Vol 1.

6. Allen, D. R., Mitchell, E. W. J., and Sinclair, R. N., "Coincidence Counting Techniques for an Epithermal Neutron Resonance DetectorSpectrometer", preprint.

7. Paoli, M. P., Mitchell, E. W. J., Sinclair, R. N., and Taylor, A. D., ICANS VIII - Proceedings of the Eighth Meeting of the International Collaboration on Advanced Neutron Sources, RAL-85-110, Rutherford Appleton Laboratory, 577-592 (1985).

8. Hughes, D. J. and Schwartz, R. B., Neutron Cross Sections, BNL 325, Second Edition, Brookhaven National Laboratory, 1958.

9. Davisson, C. M., "Gamma-Ray Attenuation Coefficients", Appendix I in Alpha-, Beta-, and Gamma-Ray Spectroscopy, Vol. 1, ed. K. Siegbahn. North-Holland, Amsterdam, 1974.

10. Blatt, J. M., and Weisskopf, V. F., Theoretical Nuclear Physics. Wiley, New York, 1952.

11. Lynn, J. E., The Theory of Neutron Resonance Reactions. Clarendon Press, Oxford, 1968.

12. Fodarero, A., The Elements of Neutron Interaction Theory. MIT Press, 1971.

13. Mughabghab, S. F. and Garber, D. I., Neutron Cross Sections, Volume I, Resonance Parameters, BNL 325, Third Edition, Brookhaven National Laboratory, 1973.

14. Motz, H., and Backstrom, G., "Neutron Capture Radiation Spectroscopy", in Alpha-, Beta-, and Gamma-Ray Spectroscopy, Vol. 1, ed. K. Siegbahn. North-Holland, Amsterdam, 1974.

15. Groshev, L. V., Demidov, A. M., and Pelekhov, V. I., Nuclear Physics 16, 645-656 (1960).

16. Strutinski, V. M., Groshev, L. V., and Akimova, M. K., Nuclear Physics 16, 657-673 (1960).

17. Bergqvist, I., and Starfelt, N., Nuclear Physics 39, 353 (1962).

18. Starfelt, N., Nuclear Physics 53, 397-408 (1964).

19. Groshev, L. V., Demidov, A. M., Pelekhov, V. I., Sokolovskii, L. L., Bartholomew, G. A., Doveika, A., Eastwood, K. M., and Monaro, S., Nuclear Data Tables A5, 243-431 (1969).

20. Davisson, C. M., "Interaction of γ-Radiation with Matter", in Alpha-, Beta-, and Gamma-Ray Spectroscopy, Vol. 1, ed. K. Siegbahn. North-Holland, Amsterdam, 1974.

21. Harshaw Scintillation Phosphors, Third Edition, The Harshaw Chemical Co., Solon OH, 1978.

22. Neiler, J. H., and Bell, P. R., "The Scintillation Method", in Alpha-, Beta-, and Gamma-Ray Spectroscopy, Vol. 1, ed. K. Siegbahn. North-Holland, Amsterdam, 1974.

23. Muradyan, G. V., Schepkin, Yu. G., Adamchuk, Yu. V., and Ustroev, G. I., Kirchatov Institute Report, IAE-2634, 22 (1979).

24. Goldstein, H., Classical Mechanics. Addison-Wesley, Reading, Mass. (1950).

25. Egelstaff, P. A., and Poole, M. J., Experimental Neutron Thermalisation. Pergamon Press, Oxford. (1969).

26. Carpenter, J. M., Potts, C. W., and Lander, G. H., ICANS-VI, Proceedings of the Sixth Meeting of the International Collaboration on Advanced Neutron Sources, ANL-82-80, Argonne National Laboratory, 78-101 (1983).

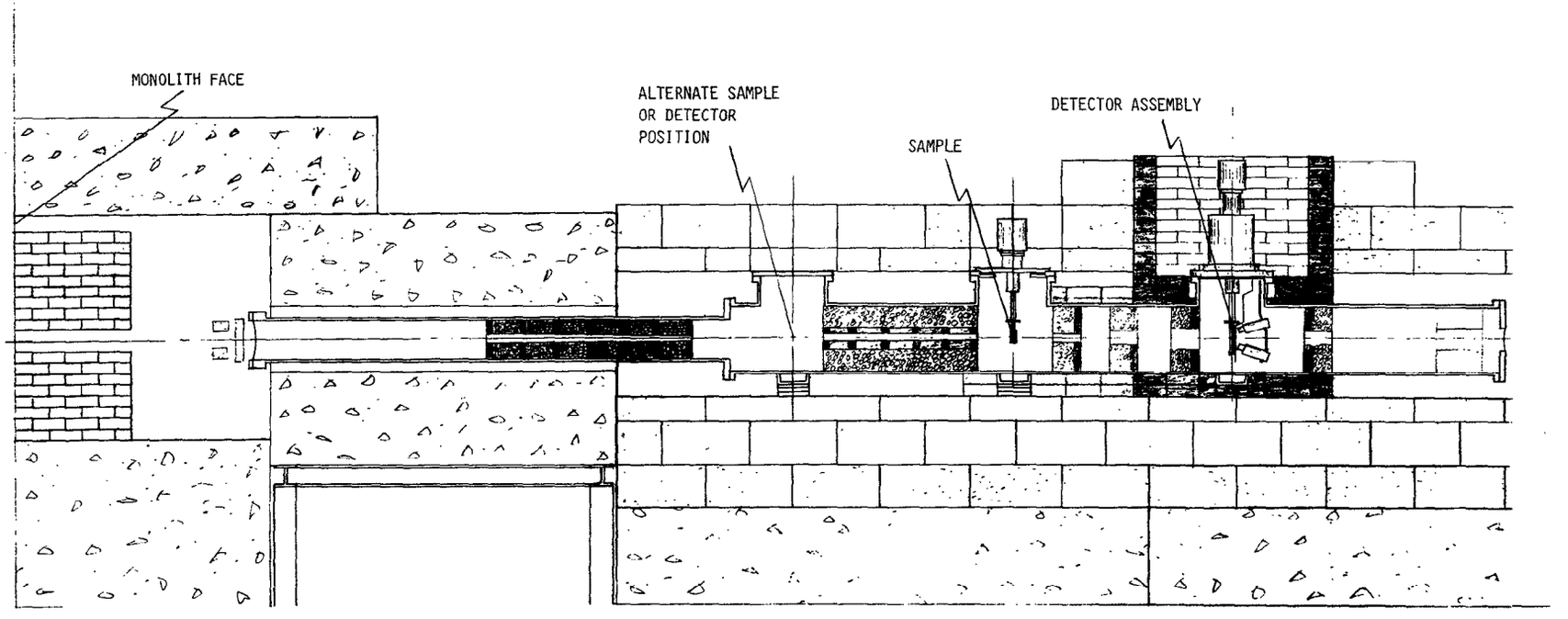

Fig. 1. Side view of the EVS flight path. The neutron beam is incident from the left. The configuration 1 detector assembly is shown. (See Table I and Figs. 2 and 3 for detector configuration specifications.)

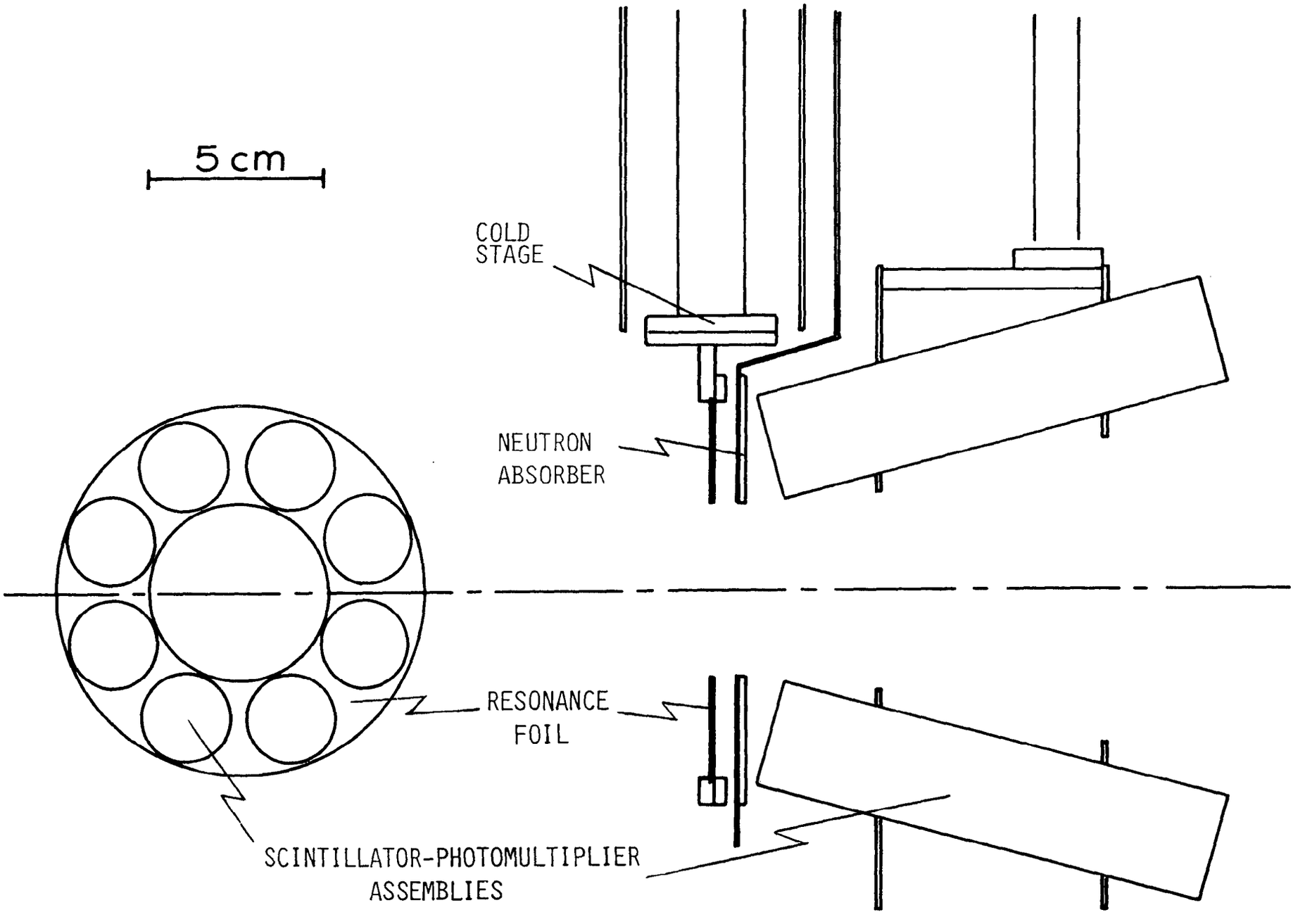

Fig. 2. Detector configuration 1. The beam is incident from the left.

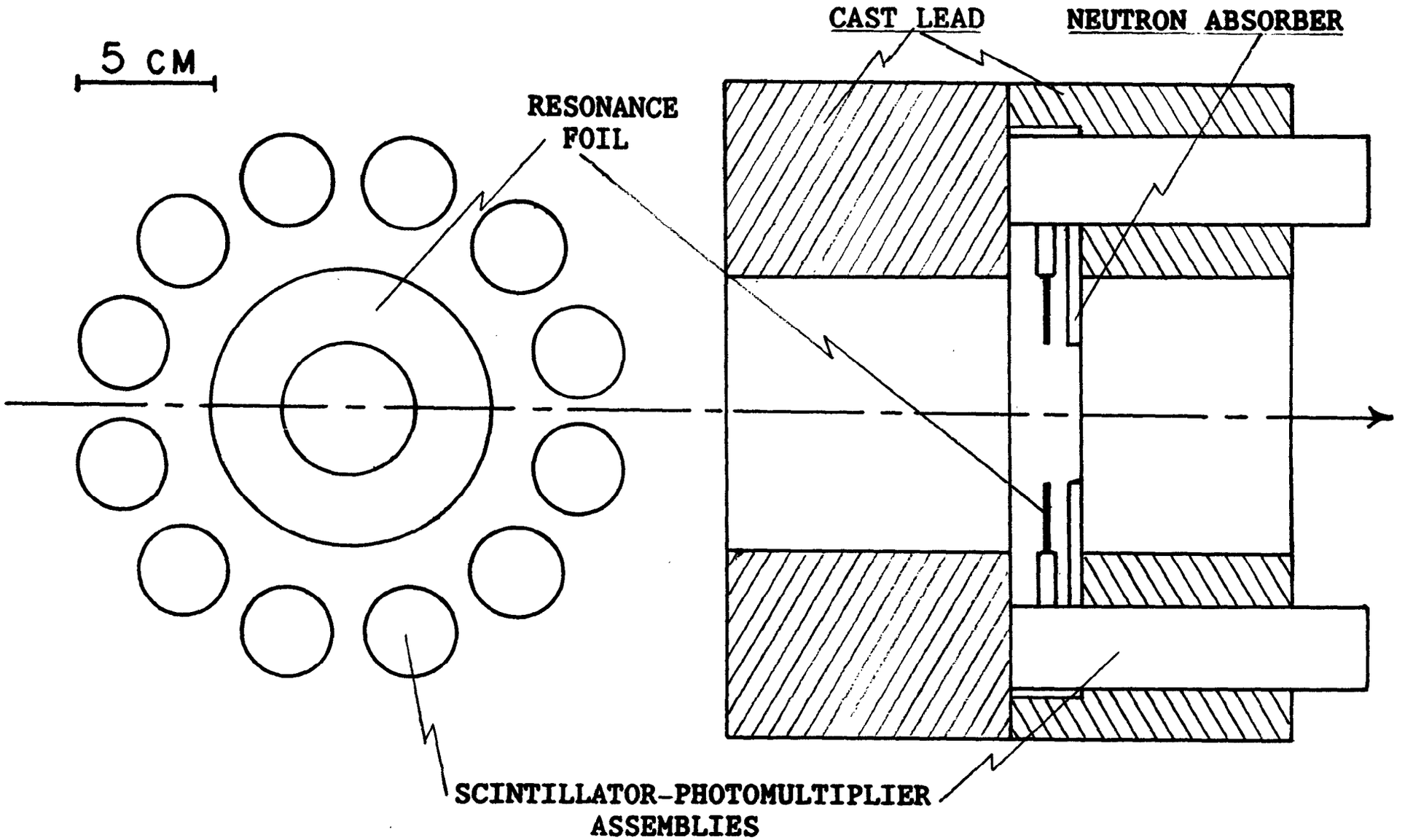

Fig. 3. Detector configuration 2. The beam is incident from the left. Only 8 of the 12 scintillator positions were occupied.

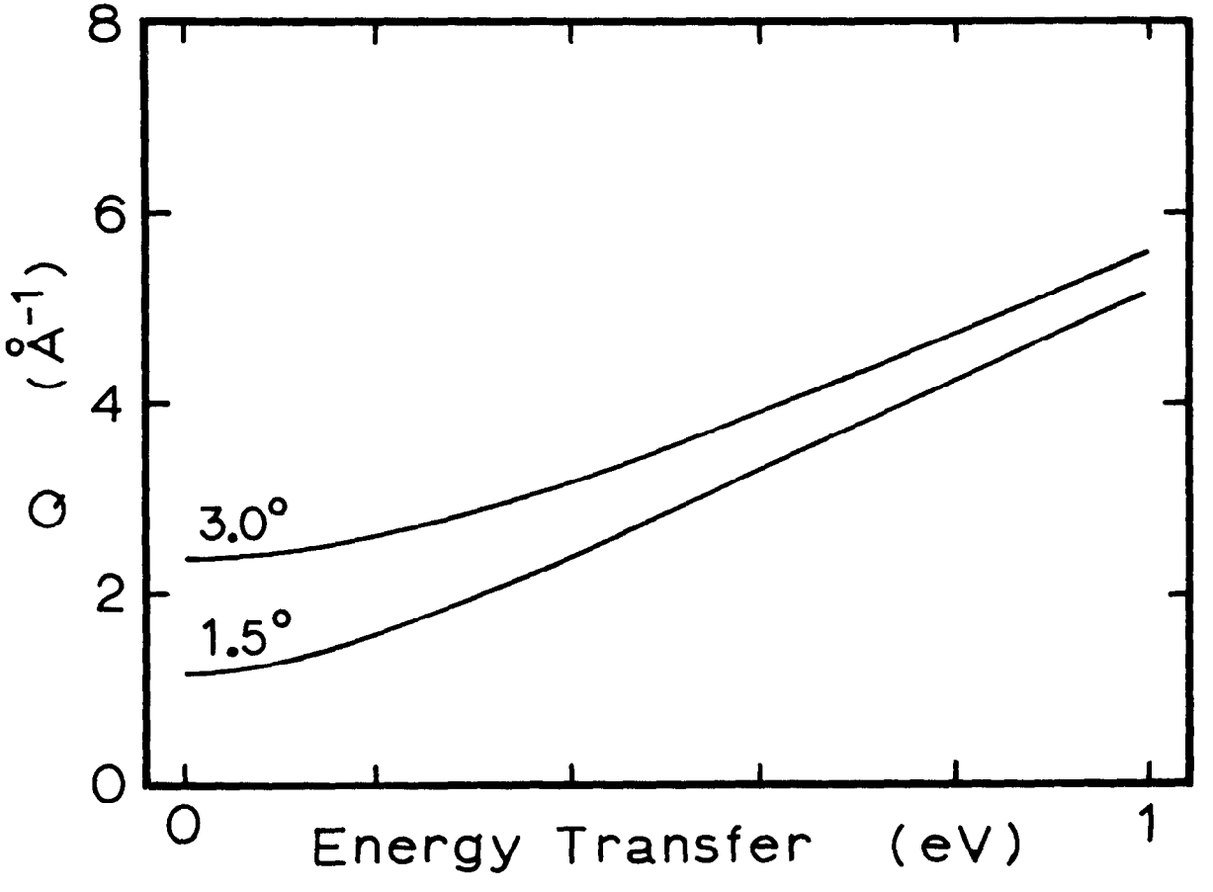

Fig. 4. Kinematic range of the detector for the EVS in configurations 1 and 2.

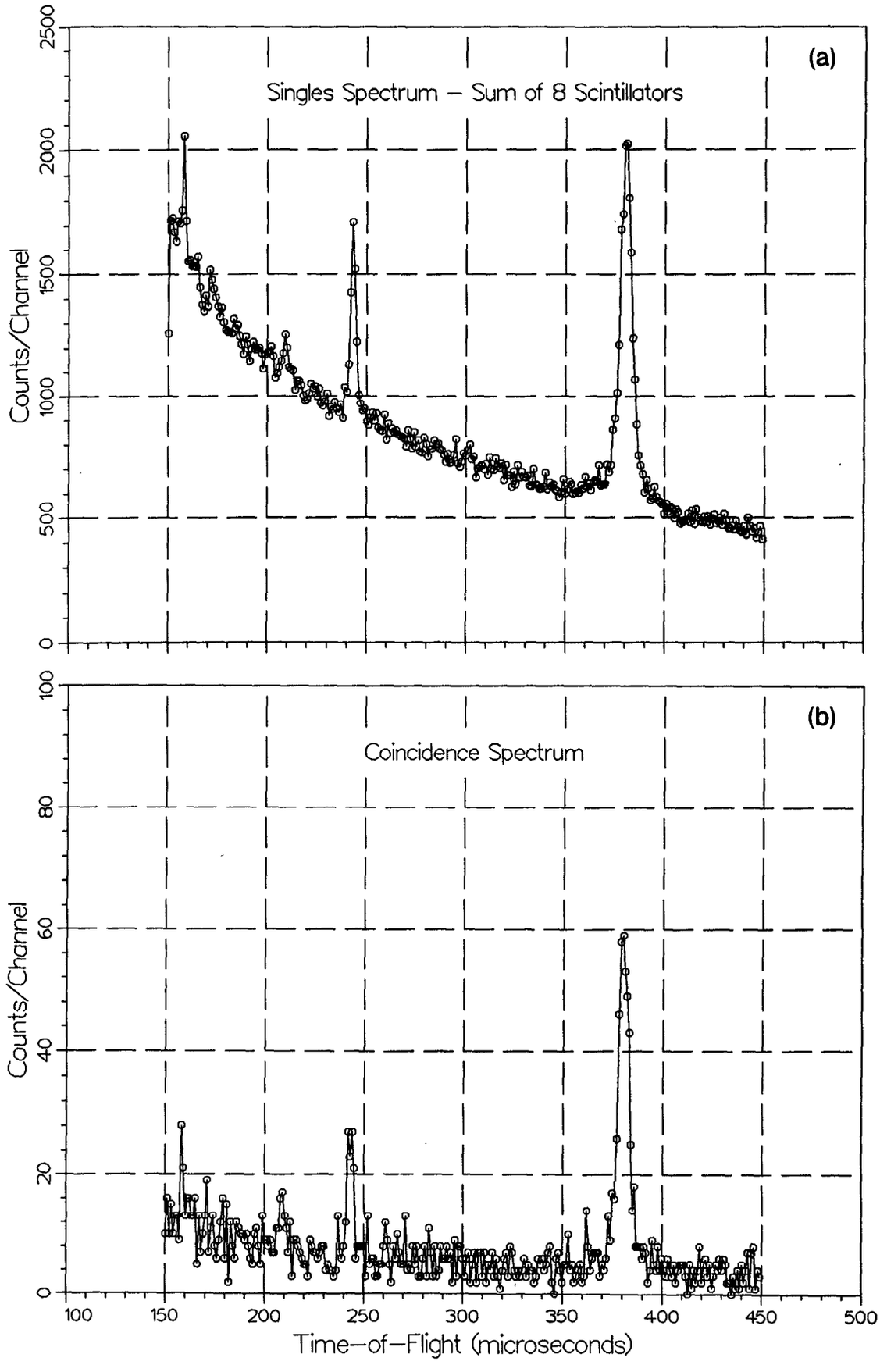

Fig. 5. Typical EVS spectra for detector configuration 1 with a polyethylene sample. (a) "Singles" spectrum sum of 8 scintillators; (b) 2-fold coincidence spectrum.

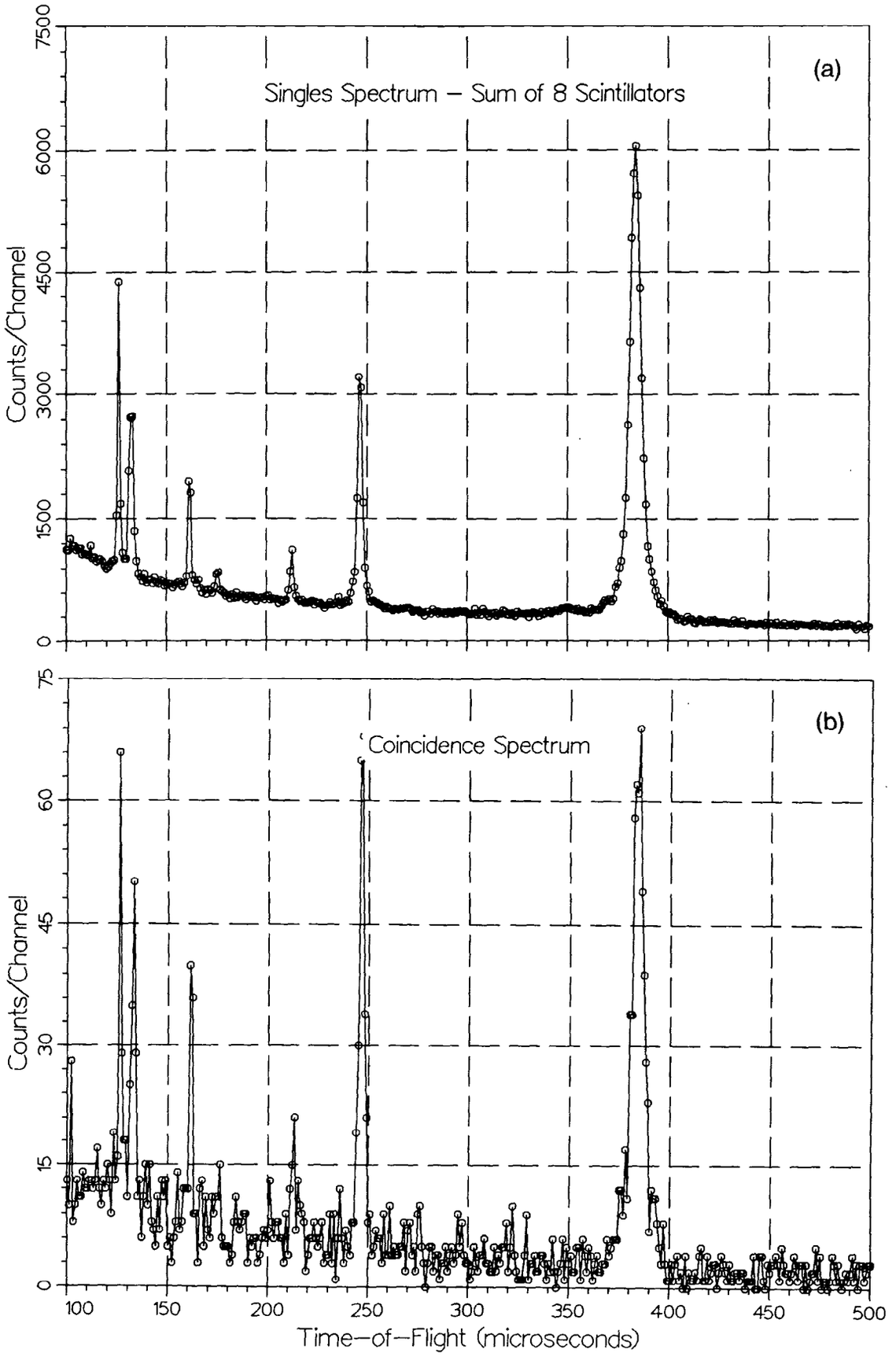

Fig. 6. Typical EVS spectra for detector configuration 2 with a polyethylene sample. (a) "Singles" spectrum sum of 8 scintillators; (b) 2-fold coincidence spectrum.

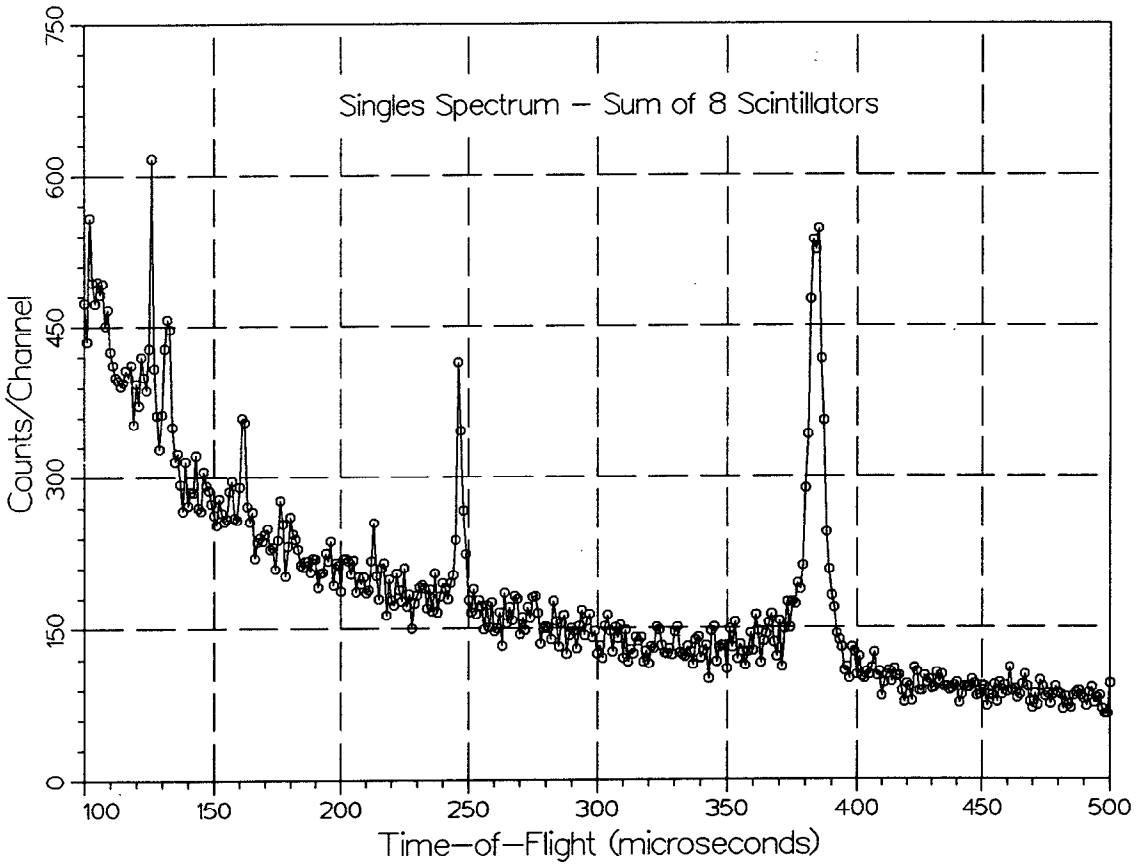

Fig. 7. Typical EVS spectrum for detector configuration 2 with a vanadium sample. "Singles" spectrum sum of 8 scintillators.

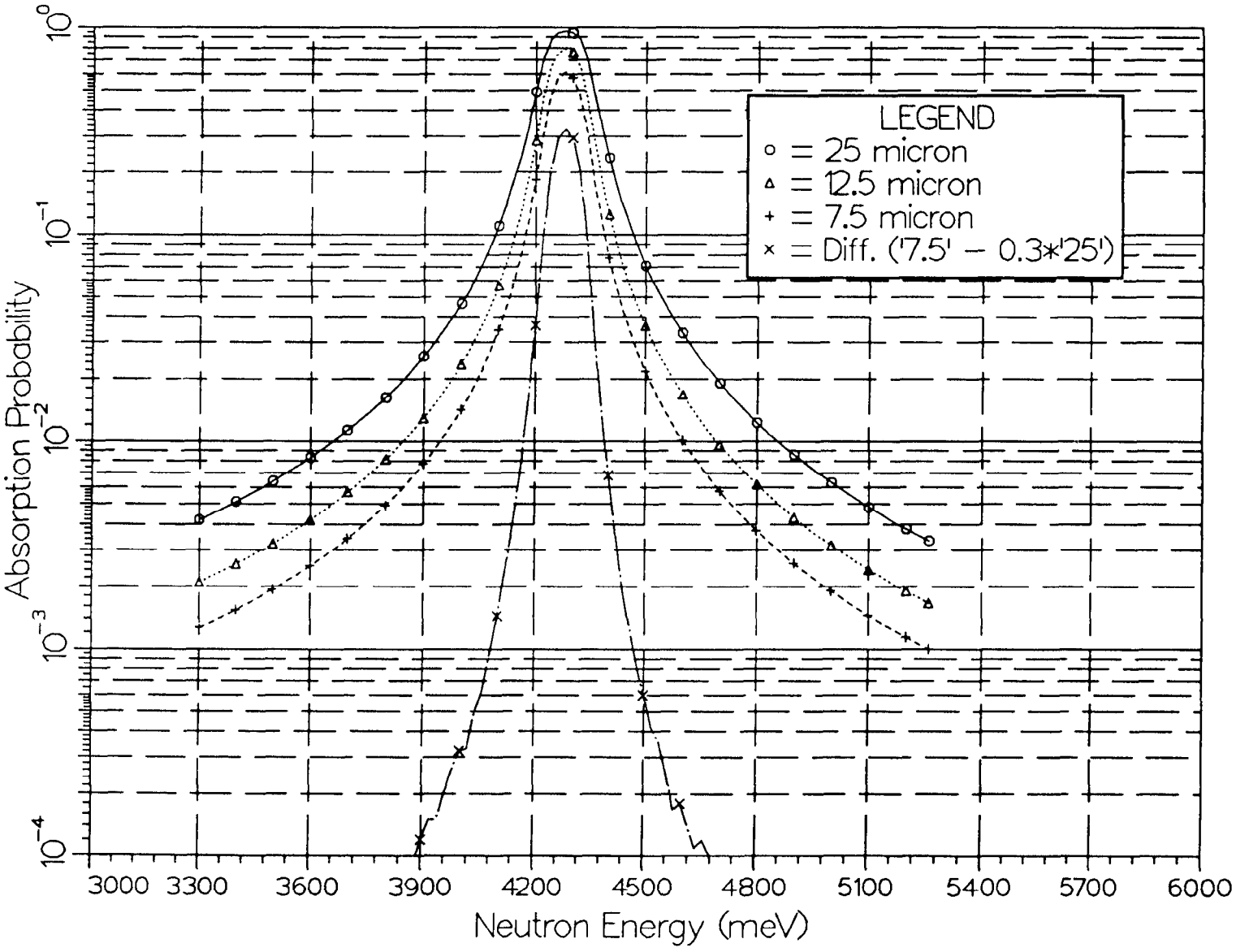

Fig. 8. Resonance absorption in Ta foil, calculated by the program FOIL. Plotted curves are absorption probabilities for 25 micron thick, 12.5 micron thick, and 7.5 micron thick foils. The difference between the 7.5 micron data and 0.3 times the 25 micron data is also plotted.

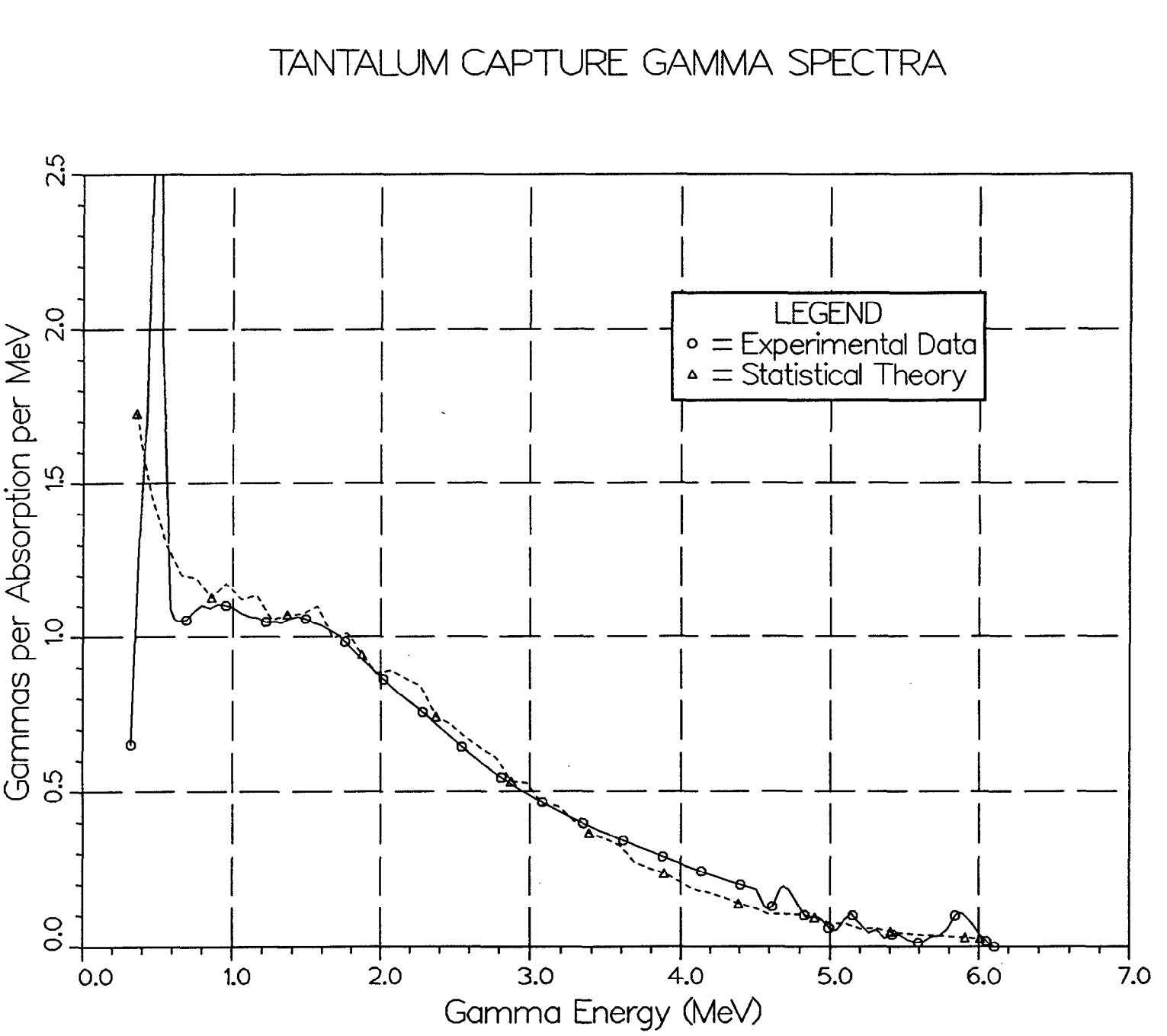

Fig. 9. Experimental (Ref. 19) and calculated capture gamma spectra for thermal neutrons on Ta. No adjustments were made in the horizontal or vertical scales for the experimental or calculated curves (numbers are absolute).

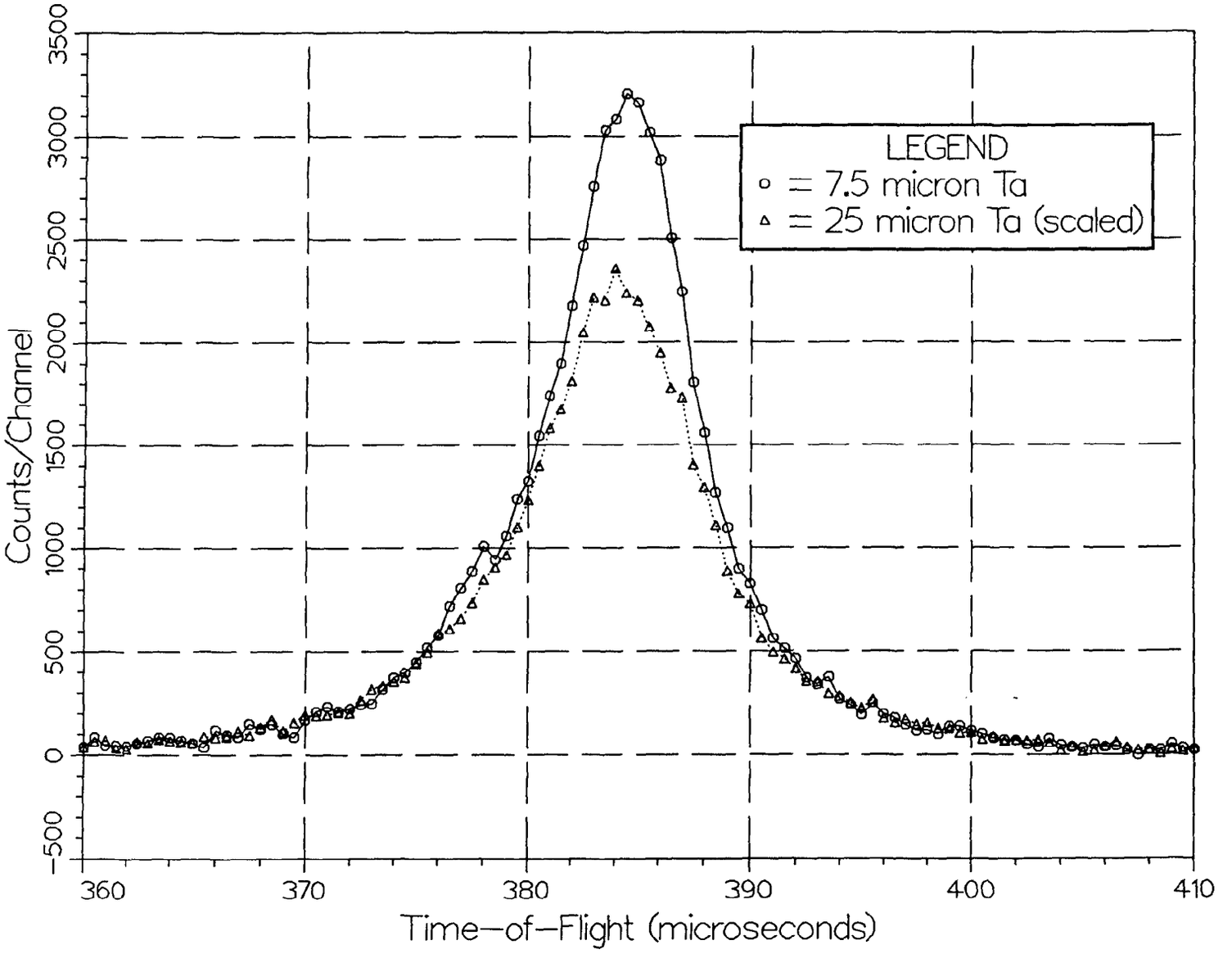

Fig. 10. Data for ZrH_2 sample near the 4280 meV elastic peak. The 7.5 micron values are the actual measured data (minus background), while the 25 micron values are the raw 25 micron data (minus background) scaled to match to match the 7.5 micron data in the wings of the Lorentzian peak.

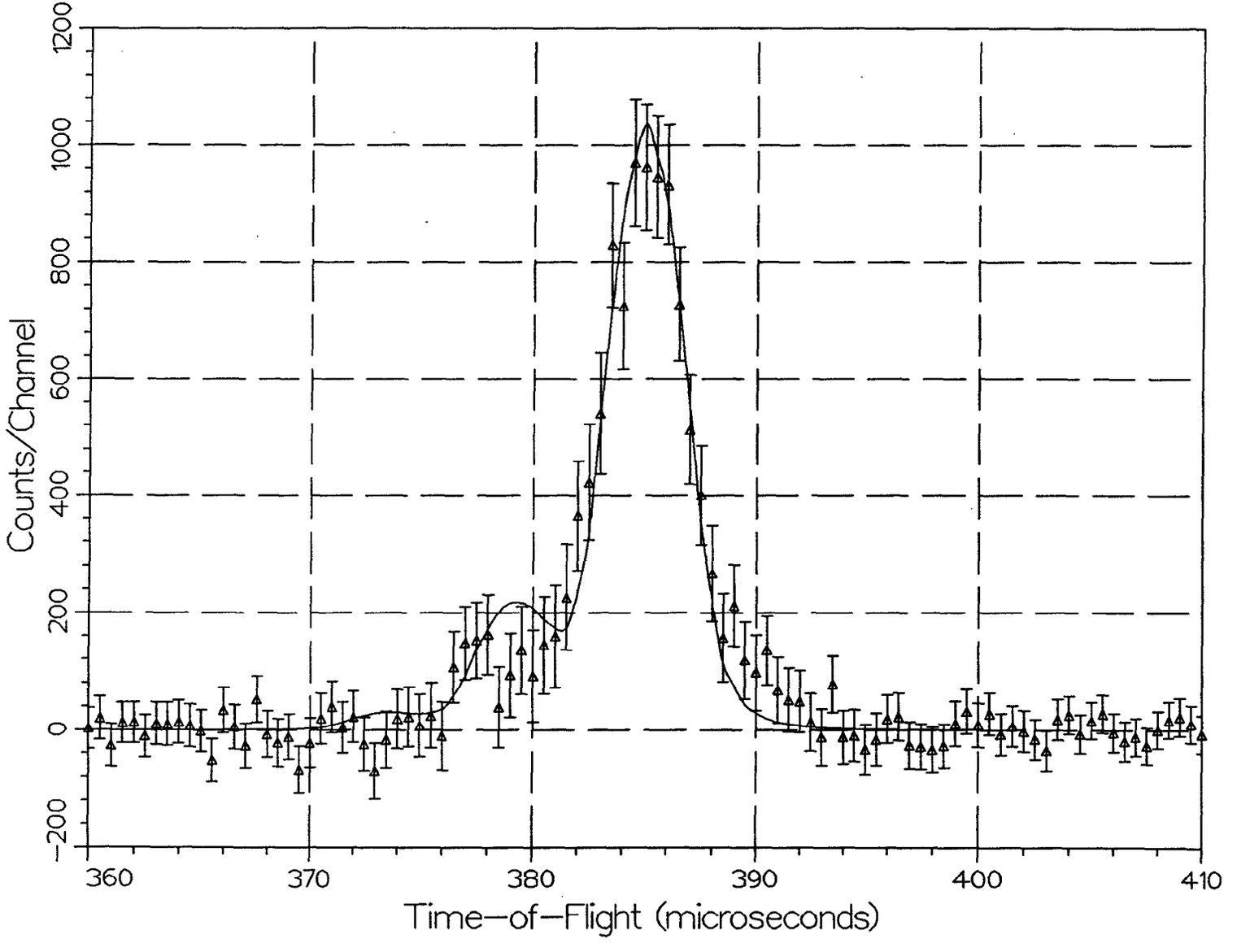

Fig. 11. "Difference" data for ZrH_2. Data points are the difference between the two curves in Fig. 10.[2] The curve is calculated using harmonic oscillator theory with an oscillator energy of 140 meV, along with the calculated difference resolution curve of Fig. 8.